W. Scherzinger
Sandia National Laboratories,
P.O. Box 5800, MS 0847,
Albuquerque, NM 87185
Mem. ASME

E. Chu
ALCOA Inc.,
Alcoa Technical Center,
Alcoa Center, PA 15069-0001
Mem. ASME

N. Triantafyllidis
Department of Aerospace Engineering,
The University of Michigan,
Ann Arbor, MI 48109-2140
Fellow ASME

Asymptotic Stability Analysis for Sheet Metal Forming—Part II: Application

The general asymptotic method proposed in Part I is applied to the investigation of the puckering instability in the hemispherical cup test. Both a membrane and a shell stress state for the principal axisymmetric solution have been considered. Due to the possibility of strong deviations from proportional loading in some cases, a corner theory of plasticity is also employed, in addition to the standard J_2 deformation theory which is often used in plastic buckling calculations. Results are compared to a previous experimental investigation for brass specimens. [S0021-8936(00)00904-1]

1 Introduction and Motivation

As an application of the general methodology of Part I, we study the puckering instability of the hemispherical cup test. The reasons for the choice of this problem are threefold: (a) relative analytical simplicity, (b) easy calculation of membrane and shell prebifurcation solutions, allowing asymptotic method to be applied to two different prestressed states, and (c) it is an interesting problem with reliable experimental data and a clear asymmetric bifurcation away from the axisymmetric principal solution.

Although our goal is not an exhaustive, in-depth study of puckering per se, a few comments are in order concerning the hemispherical cup test. In addition to its practical interest as a benchmark test for the appearance of wrinkles around corners in sheet metal forming (see Devons [1]), the problem possesses a very interesting theoretical aspect (see Triantafyllidis [2]): unlike most plastic buckling problems that are studied, which have a proportional loading path (beams, plates, cylinders), the hemispherical cup test has large deviations from proportional loading. This feature has implications concerning the constitutive model that is used. The goal here is to show the validity of the asymptotic methodology presented in Part I and to compare the results found using a membrane theory prestress and a shell theory prestress. In addition we investigate, in a systematic fashion, the influence of the constitutive theory and the friction boundary conditions.

The presentation of the work begins with the formulation of the problem in Section 2. The kinematics for the axisymmetric principal solution are given first, followed by the stability functional for the hemispherical cup test as deduced from the general theory of Part I. Finally, a brief discussion of numerical considerations concludes the problem formulation. In Section 3 numerical results based on the above derived stability functional are compared to the experimental data of Donoghue et al. [3] for the hemispherical cup test performed on circular brass disks. The effect of sheet thickness on the loading history is examined, and as a result, the effect of the choice of the constitutive theory on the critical height is also considered. Finally, the influence of the boundary conditions, arising from the friction between the tooling surfaces and the sheet is also investigated.

Contributed by the Applied Mechanics Division of THE AMERICAN SOCIETY OF MECHANICAL ENGINEERS for publication in the ASME JOURNAL OF APPLIED MECHANICS. Manuscript received by the ASME Applied Mechanics Division, Sept. 24 1999; final revision, Jan. 30 2000. Associate Technical Editor: S. Kyriakides. Discussion on the paper should be addressed to the Technical Editor, Professor Lewis T. Wheeler, Department of Mechanical Engineering, University of Houston, Houston, TX 77204-4792, and will be accepted until four months after final publication of the paper itself in the ASME JOURNAL OF APPLIED MECHANICS.

2 Problem Formulation

The application of the general methodology of Part I to the hemispherical cup puckering test requires the solution of the axisymmetric sheet punching problem. For this solution, two cases are considered: a membrane theory and a shell theory prestress. The membrane theory is an approximate solution, while the shell theory (see Triantafyllidis and Samanta [4]) is a consistent finite rotation and finite strain shell theory with a more accurate prestress.

Following the presentation of the kinematics and of the bifurcation functional for the problem at hand, there is a brief discussion of numerical considerations for the finite element discretization of the problem and the calculation of the critical punch height.

As mentioned in the Introduction, the choice of constitutive response is very important for plastic buckling problems. Due to nonproportional loading of the principal solution, the present stability calculations use the corner theory of Christoffersen and Hutchinson [5]. This theory gives the flexibility of investigating a range of constitutive theories from deformation theory to flow theory.

2.1 Kinematics. The geometry of the hemispherical cup test is shown in Fig. 1 while the kinematics for the undeformed and deformed configurations are shown in Fig. 2. For an axisymmetric sheet the convected coordinates θ^i are used, where $\theta^1=s$, $\theta^2=\theta$, and $\theta^3=z$. The meridian for the surface of revolution that describes the midsurface of the sheet in the undeformed configuration is depicted by the line $\mathcal{C}$ in Fig. 2. A material point on the midsurface is given by its position vector $\mathbf{R}$, and an arbitrary material point, at distance z from the midsurface, is given by $\mathbf{P}$

$$P(s,\theta,z)=\mathbf{R}(s,\theta)+z\mathbf{N}(s,\theta), \quad -\frac{h}{2}\leqslant z\leqslant\frac{h}{2}, \tag{2.1}$$

where $\mathbf{N}$ is the unit normal to the midsurface at $\mathbf{R}$. During the deformation of the initially flat sheet, a point on the midsurface initially at $\mathbf{R}$, undergoes a displacement $\mathbf{u}$ and its new position on the deformed midsurface, depicted by curve $\bar{\mathcal{C}}$ in Fig. 2, is given by $\mathbf{r}=\mathbf{R}+\mathbf{u}$. The position vector for an arbitrary material point, at distance $\bar{z}$ from the midsurface, is given by $\mathbf{p}$,

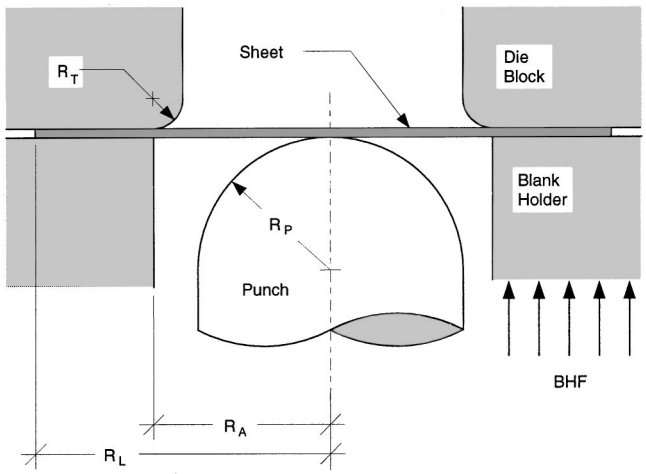

Fig. 1 Schematic drawing for hemispherical cup test

$$\mathbf{p}(s,\theta,z)=\mathbf{r}(s,\theta)+\overline{z}\mathbf{n}(s,\theta),\quad -\frac{\overline{h}(s)}{2}\leqslant\overline{z}\leqslant\frac{\overline{h}(s)}{2},\quad (2.2)$$

where $\mathbf{n}$ is the unit normal to the current midsurface at $\mathbf{r}$ and $\overline{h}(s)$ is the current sheet thickness. The displacement, $\mathbf{u}$, has components $v(s)$ and $w(s)$ along the radial and axial directions, respectively, i.e.,

$$\mathbf{u}(s,\theta)=v(s)\mathbf{e}_r(\theta)+w(s)\mathbf{e}_3;\quad \mathbf{e}_r(\theta)=\cos\theta\mathbf{e}_1+\sin\theta\mathbf{e}_2. \quad (2.3)$$

The basis vectors for the midsurface in the current configuration, $\mathbf{a}_i$, expressed in terms of the local orthonormal basis $\{\mathbf{t},\mathbf{n},\mathbf{b}\}$, are

$$\mathbf{a}_1=\frac{\partial\mathbf{r}}{\partial s}=\lambda_s\mathbf{t},\quad \mathbf{a}_2=\frac{\partial\mathbf{r}}{\partial\theta}=\rho\mathbf{b},\quad \mathbf{a}_3=\mathbf{n}, \quad (2.4)$$

where $\mathbf{t}$ is the unit tangent to the curve $\overline{\mathcal{C}}$, λ_s is the radial stretch ratio and ρ is the current distance from the axis of symmetry, which are found with the help of (2.1)–(2.4) to be

$$\lambda_s=\frac{d\tilde{s}}{ds}=\left[\left(1+\frac{dv}{ds}\right)^2+\left(\frac{dw}{ds}\right)^2\right]^{1/2},\quad \rho=s+v(s). \quad (2.5)$$

From differential geometry (e.g., Goetz [6]), the nonzero components of the curvature tensor for the axisymmetric midsurface are

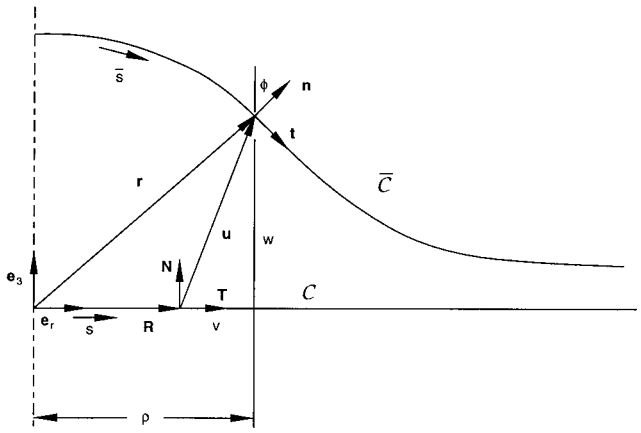

Fig. 2 Kinematics for axisymmetric shell and membrane theories. $\mathcal{C}$ is the meridian for the sheet in the undeformed (reference) configuration, and $\bar{\mathcal{C}}$ is the meridian for the sheet in the deformed (current) configuration.

$$b_1^1=-k_s=\frac{1}{\lambda_s^2}\left(\sin\phi\frac{d^2v}{ds^2}+\cos\phi\frac{d^2w}{ds^2}\right),\quad b_2^2=-k_\theta=-\frac{\sin\phi}{\rho} \quad (2.6)$$

where $\cos\phi=\mathbf{N}\cdot\mathbf{n}$. The nonzero Christoffel symbols for the current midsurface are found from Eq. (2.5) in Part I

$$t_{11}^1=\frac{1}{\lambda_s}\frac{d\lambda_s}{ds},\quad t_{12}^2=t_{21}^2=\frac{1}{\rho}\frac{d\rho}{ds},\quad t_{22}^1=-\frac{\rho}{\lambda_s^2}\frac{d\rho}{ds}. \quad (2.7)$$

With these kinematic quantities, the stability functional presented in Part I can be evaluated for the axisymmetric hemispherical cup test.

2.2 Stability Functional. Using the results from Part I, and representing tensor quantities with their physical components,[1] the stability functional for an axisymmetric shell is according to Eq. (3.24) in Part I

$$\mathcal{F}(\overset{0}{\overline{v}}_{\langle i\rangle};H)=\frac{1}{2}\int_A\left\{\int_{-h/2}^{h/2}[\overline{\mathcal{P}}^{\langle i\beta k\delta\rangle}\hat{v}_{\langle k,\delta\rangle}\hat{v}_{\langle i,\beta\rangle}\mu]dz+[\hat{K}^{\langle ik\rangle}\hat{v}_{\langle k\rangle}\hat{v}_{\langle i\rangle}]_{\theta^3=-h/2}\right\}dA, \quad (2.8)$$

where $\hat{v}_{\langle i\rangle}$ is deduced from Eq. (3.25) of Part I under the assumption $\langle\overset{1}{\overline{\mathcal{P}}}_{i\beta k\delta}\rangle\approx 0$,

$$\hat{v}_{\langle i\rangle}=\overset{0}{\overline{v}}_{\langle i\rangle}-\theta^3(L^{\langle m3i3\rangle})^{-1}L^{\langle m3k\delta\rangle}\left[\frac{\partial\overset{0}{\overline{v}}_{\langle k\rangle}}{\partial\theta^\delta}-t_{k\delta}^r\overset{0}{\overline{v}}_{\langle r\rangle}\right], \quad (2.9)$$

and the incremental moduli, appearing in (2.9) (and in the expression for the plane stress moduli $\mathcal{P}$), are given in Triantafyllidis [2]. For simplicity, we introduce the notation $\overset{0}{\overline{v}}_{\langle 1\rangle}\equiv\overline{u}$, $\overset{0}{\overline{v}}_{\langle 2\rangle}\equiv\overline{v}$ and $\overset{0}{\overline{v}}_{\langle 3\rangle}\equiv\overline{w}$. Using the kinematics from Section 2.1 in conjunction with (2.9), the plane stress assumption and the axisymmetry of the stress state, the strain rate terms $\hat{v}_{\langle i,j\rangle}$ in (2.8) are found to be

$$\hat{v}_{\langle 1,1\rangle}=\frac{1}{\lambda_s(1+k_s\overline{z})}\left\{\frac{\partial\overline{u}}{\partial s}-\lambda_s k_s\overline{w}-\overline{z}\left(\frac{\partial\alpha}{\partial s}\right)\right\} \quad (2.10)$$

$$\hat{v}_{\langle 1,2\rangle}=\frac{1}{\rho(1+k_\theta\overline{z})}\left\{\frac{\partial\overline{u}}{\partial\theta}-\overline{v}\cos\phi-\overline{z}\left(\frac{\partial\alpha}{\partial\theta}-\beta\cos\phi\right)\right\} \quad (2.11)$$

$$\hat{v}_{\langle 2,1\rangle}=\frac{1}{\lambda_s(1+k_s\overline{z})}\left\{\frac{\partial\overline{v}}{\partial s}-\overline{z}\left(\frac{\partial\beta}{\partial s}\right)\right\} \quad (2.12)$$

$$\hat{v}_{\langle 2,2\rangle}=\frac{1}{\rho(1+k_\theta\overline{z})}\left\{\frac{\partial\overline{v}}{\partial\theta}+\overline{u}\cos\phi+\overline{w}\sin\phi-\overline{z}\left(\frac{\partial\beta}{\partial\theta}+\alpha\cos\phi\right)\right\} \quad (2.13)$$

$$\hat{v}_{\langle 3,1\rangle}=\alpha;\quad \hat{v}_{\langle 3,2\rangle}=\beta \quad (2.14)$$

where for simplicity, the following auxiliary quantities α and β have been introduced:

$$\alpha\equiv\frac{1}{\lambda_s}\frac{\partial\overline{w}}{\partial s}-k_s\overline{u},\quad \beta\equiv\frac{1}{\rho}\frac{\partial\overline{w}}{\partial\theta}-k_\theta\overline{v}. \quad (2.15)$$

Finally, it is noted that the stability functional in (2.8) can be used with a membrane or shell prestressed state. A membrane prestress state, one with no bending stiffness, gives a stress field that is constant through the thickness of the sheet, resulting in plane stress incremental moduli that depend solely on the midsurface coordinate s. On the other hand, a shell prestress state gives a

[1]The physical components of a tensor are denoted with the subscripts or superscripts of the tensor enclosed in brackets $\langle\cdot\rangle$.

varying stress state through the thickness of the sheet, in which case the plane stress incremental moduli are integrated through the sheet thickness.

2.3 Numerical Considerations. The methodology and algorithm for calculating the axisymmetric principal solutions is presented in detail in Triantafyllidis [2] for the membrane model and Triantafyllidis and Samanta [4] for the shell model, respectively. The same references also contain detailed derivations of the incremental moduli for the deformation and corner theory constitutive models employed here. The determination of the positive definiteness of the stability functional is done by employing the same finite element discretization used for the principal solution. The axisymmetry of the principal solution, suggests a Fourier decomposition for the eigenmode

$$\overline{u}(s,\theta)=\sum_{n=0}^{\infty}\left[u_n^*(s)\cos(n\theta)+u_n(s)\sin(n\theta)\right], \tag{2.16}$$

$$\overline{v}(s,\theta)=\sum_{n=0}^{\infty}\left[v_n(s)\cos(n\theta)+v_n^*(s)\sin(n\theta)\right], \tag{2.17}$$

$$\overline{w}(s,\theta)=\sum_{n=0}^{\infty}\left[w_n^*(s)\cos(n\theta)+w_n(s)\sin(n\theta)\right], \tag{2.18}$$

where $n\geqslant 1$ is the eigenmode's wave number. Using (2.16)–(2.18) and exploiting the orthogonality of the trigonometric functions, the stability functional can be written as

$$\mathcal{F}(\overline{u},\overline{v},\overline{w};H)=\sum_{n=1}^{\infty}\left[\mathcal{F}_n(u_n(s),v_n(s),w_n(s))+\mathcal{F}_n(u_n^*(s),v_n^*(s),w_n^*(s))\right], \tag{2.19}$$

where $\mathcal{F}_n$ are quadratic functionals of the three s-dependent parts of the eigenmode $(u_n(s),v_n(s),w_n(s)$, or equivalently of $u_n^*(s),v_n^*(s),w_n^*(s))$ and the wave number n. By inspection of (2.19), it is seen that loss of positive definiteness of some $\mathcal{F}_n$, results in loss of positive definiteness of $\mathcal{F}$. Hence the stability analysis of the two-dimensional puckering problem is reduced to the determination of positive definiteness of a one-dimensional stability functional over a given range of wave numbers n, thus greatly simplifying the analysis.

For assembling the stability functional $\mathcal{F}_n$, we use the same mesh as for the principal axisymmetric solution but with a linear interpolation function for $\overline{u},\overline{v}$ and a Hermitian cubic interpolation for $\overline{w}$. A Cholesky decomposition of the resulting symmetric stiffness matrix $\mathbf{K}_n$ is used, i.e., $\mathbf{K}_n=\mathbf{L}_n\mathbf{D}_n\mathbf{L}_n^T$. For a given punch height, the stability of the structure is examined by looking at the sign of the minimum entry in diagonal matrix $\mathbf{D}_n$ over a large range of integers n (typically from 1 to 25). The critical height H_c is the lowest punch displacement at which this entry becomes negative for some integer n.

3 Results

The goal of this section is to compare the predictions of the theory derived in Section 2 with experimental results and also to examine the accuracy of the membrane prestress simplification, as opposed to the shell theory prestress, for the prediction of the critical punch height. The experimental results used in our comparisons were performed by Donoghue et al. [3] where circular brass blanks of four different thicknesses, h, of 0.508 mm, 0.635 mm, 0.813 mm, and 1.016 mm, were tested. In addition to varying the sheet thickness, the tooling size and draw ratio (R_L/R_A) were also varied. Results will be presented here for two tooling sizes, S_1 and S_2, (shown in Table 1) and for two draw ratios $(R_L/R_A=1.7$ and $R_L/R_A=1.5)$.

Table 1 Tooling sizes used in Donoghue et al. [3]

	S_1	S_2
R_P	50.00 mm	33.33 mm
R_A	58.33 mm	38.87 mm
R_T	10.71 mm	6.94 mm

Experimental data for the brass uniaxial stress-strain curves closely follow a bilinear hardening model. The initial elastic modulus is $E=110$ GPa. For the three thinest sheets the yield stress is $\sigma_y=195$ MPa and the tangent modulus is $E_t=812$ MPa, while for the thickest sheet, $h=1.016$ mm, the yield stress is $\sigma_y=120$ MPa, and the tangent modulus is $E_t=852$ MPa. For the brass experiments there was no measured plastic anisotropy in the sheets.

Considerable effort was devoted to removing the effects of friction in the tests reported by Donoghue et al. [3] by using teflon sheets between the blank and the tooling, and the friction coefficient between the tooling and the sheet, while not removed entirely, was reduced considerably. The value $\mu=0.04$ used in the simulations reported in Donoghue et al. [3], has also been used for all numerical calculations in this work.

To constrain wrinkling in the flange, a blank holder force (BHF) was applied to the sheet between the blank holder and the die block. Table 2 shows the blank holder forces for all of the experimental cases examined here.

For all comparisons between the experimental and theoretical results, J_2 deformation theory of plasticity is used, which gives a lower bound on the critical punch height. The influence of the constitutive response of the material is examined later. Note that all subsequent comparisons involve the critical height, which is very sensitive to the constitutive description employed. The critical wave number, being determined mainly by geometry, is always in good agreement with experimental results, as discussed by Donoghue et al. [3] and hence is of no further concern.

For the first set of comparisons, the largest tooling (S_1) is used and the draw ratio is $R_L/R_A=1.7$. The results for this case are shown in Table 3. For thin sheets the theoretical predictions using both the shell and membrane theories, show good agreement with the experimental results. The percent error for the 0.508 mm sheet is 2.2 percent using the shell theory and 13.7 percent with the membrane theory. As the sheet thickness increases the theoretical predictions using the deformation theory grow progressively worse. For the 1.016-mm sheet, the shell theory result underpredicts the critical punch height by 36.5 percent, while for the membrane theory calculation the error is 48.4 percent. The main reason for this discrepancy lies in the large deviations from proportional loading that occur. For the thickest sheets the deviations from

Table 2 Blankholder force (BHF) for cases examined in experimental study by Donoghue et al. [3]

Tooling	R_L/R_A	Thickness (mm)	BHF (kN)	Tooling	R_L/R_A	Thickness (mm)	BHF (kN)
S1	1.7	0.508	34.637	S1	1.5	0.635	33.373
S1	1.7	0.635	33.809	S1	1.5	0.813	33.818
S1	1.7	0.813	41.227	S1	1.5	1.016	41.320
S1	1.7	1.016	41.316	S2	1.7	0.508	49.570
S1	1.5	0.508	33.168	S2	1.7	0.635	49.837

Table 3 Experimental and theoretical results using deformation theory with $R_L/R_A=1.7$ and the S_1 tooling

Thickness	0.508 mm	0.635 mm	0.813 mm	1.016 mm
H_c (experimental)	22.86 mm	29.46 mm	36.38 mm	54.36 mm
H_c (shell theory)	22.35 mm	25.15 mm	30.81 mm	34.54 mm
H_c (membrane theory)	19.72 mm	21.15 mm	24.64 mm	28.05 mm

Table 4 Experimental and theoretical results using deformation theory with $R_L/R_A=1.5$ and the S_1 tooling

Thickness	0.508 mm	0.635 mm	0.813 mm	1.016 mm
H_c (experimental)	13.46 mm	18.03 mm	24.38 mm	41.91 mm
H_c (shell theory)	13.72 mm	15.81 mm	19.02 mm	24.18 mm
H_c (membrane theory)	13.37 mm	15.37 mm	18.06 mm	22.15 mm

proportional loading are larger, especially for material points away from the midsurface of the sheet. As a result the deformation theory of plasticity will not be as accurate for the thicker sheets. This point will be addressed subsequently.

Next attention is turned to experiments run with the same tooling as before (S_1), but with a smaller draw ratio of $R_L/R_A=1.5$. The experimental and theoretical results for this case are shown in Table 4. It is seen, as in the previous case, that the predictions for thin sheets, using J_2 deformation theory, are very good, while those for thick sheets are not as accurate. For the 0.508-mm sheet the percent error, using both the shell and membrane theories, is under 2.0 percent. But as the sheet thickness increases, once again the error grows quite large. For the 1.016-mm sheet the percent error is 42.3 percent for the shell theory and 47.1 percent for the membrane theory.

Results are also examined for tests run with a smaller tooling, S_2, which gives higher curvatures, and a draw ratio of $R_L/R_A=1.7$. These results are shown in Table 5. Here it is seen, as in the previous cases, that the shell theory performs better than the membrane theory when estimating the critical punch height. The larger curvatures in this problem, especially near the die throat, necessitate a shell theory. (Experiments using the 0.813-mm and 1.016-mm sheets were not performed by Donoghue et al. [3].)

The role of the constitutive theory in plastic buckling problems is extremely important and is often the major reason for the discrepancy between theoretical buckling calculations and experimental observations (see review article by Hutchinson [7]). For most commonly studied problems, the prebuckling solution has proportional loading, and deformation theory of plasticity will predict the instability. However, in the problem examined here, large deviations from proportional loading occur, especially for the thickest sheets. Deformation theory is inadequate when large deviations from proportional loading occur, and as a result, it is not expected to accurately predict instabilities for thicker sheets.

To examine the effect of sheet thickness on the deviation from proportional loading, we follow the stress histories for material points in the unsupported region of the cup, which lie initially near the die throat. This choice is dictated by the fact that the stress distribution in the unsupported region, has the greatest effect on the stability calculations. Presented here are the stress histories for the thinest sheet, 0.508 mm, and the thickest sheet, 1.016 mm, using the largest tooling and a draw ratio of $R_L/R_A=1.7$. The stress history for material points in the 0.508-mm sheet, at an initial radius of 48.12 mm are shown in Fig. 3. This point in the sheet has a location in the unsupported region of the sheet when the punch reaches H_c and the resultant hoop force at this point is compressive. The yield surface is plotted in $\sigma_{11}-\sigma_{22}$ space. Material points on the top, middle, and bottom surface load through the elastic range, reach the yield surface, and continue loading in the plastic range. For the middle surface there is not a strong deviation from proportional loading after yield. The top and bottom surfaces, however, do show strong deviations from proportional loading after yielding has occurred. Notice, however, that the corresponding stresses are just out of the initial yield surface.

These results are compared to the stress histories for the thickest sheet, $h=1.016$ mm, shown in Fig. 4. Again the stress histories are plotted for a material point at an initial radius of 48.12 mm. Here large deviations from proportional loading are seen throughout the sheet and the stresses are now deeply into the plastic range. The stresses in the sheet are redistributed after yielding in order to sustain equilibrium, and this stress redistribution is greater if the sheet is thicker, resulting in larger deviations from proportional loading. Nearly proportional loading is necessary for the accuracy of a deformation theory, and as a result, the plasticity theory chosen to model the behavior of the thinner sheets, i.e., deformation theory, is not necessarily valid for the thicker sheets. To improve on the deformation theory, a corner theory is employed to predict buckling.

The effect of sheet thickness on the critical punch height for

Table 5 Experimental and theoretical results using deformation theory with $R_L/R_A=1.5$ and the S_2 tooling

Thickness	0.508 mm	0.635 mm
H_c (experimental)	34.80 mm	38.86 mm
H_c (shell theory)	30.18 mm	31.32 mm
H_c (membrane theory)	21.09 mm	22.23 mm

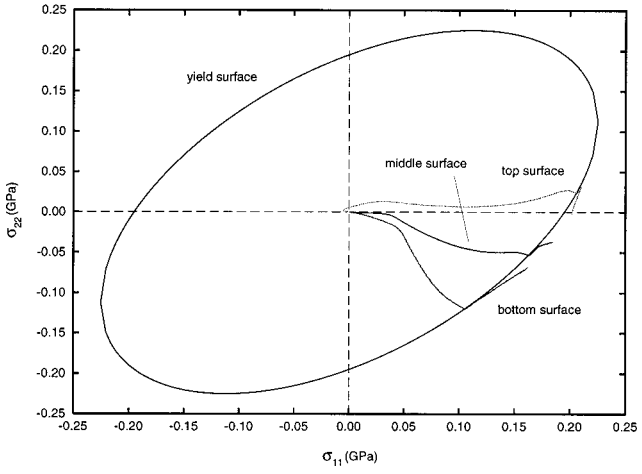

Fig. 3 Stress history for material points initially at a radius of 48.12 mm for the 0.508 mm sheet. Stress history is shown for the bottom, middle, and top surfaces of the shell.

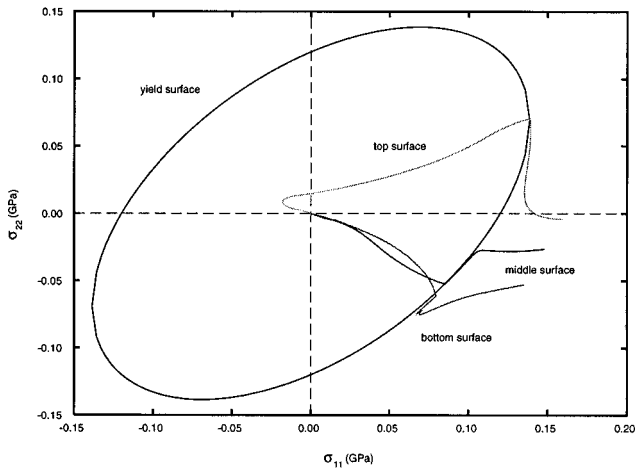

Fig. 4 Stress history for material points initially at a radius of 48.12 mm for the 1.016 mm sheet. Stress history is shown for the bottom, middle and top surfaces of the shell.

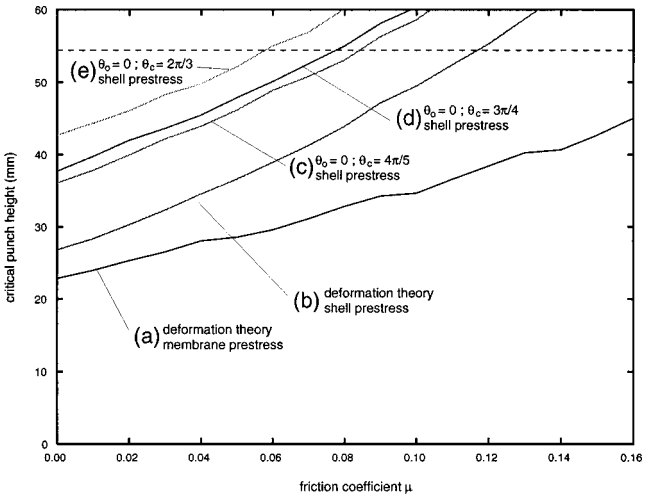

Fig. 6 Effect of friction on the critical punch height for 1.016 mm brass sheet with $R_L/R_A=1.7$, the S_1 tooling and a BHF $=41.316$ kN. The trend in the results is the same as that seen in Fig. 5, and it shows the great dependence of the results on the friction boundary conditions, which are often difficult to measure. The experimental result for this case is shown by the dashed line.

various corner theories can be seen in Fig. 5. The coefficient of friction for all the cases shown is 0.04 and the BHF is 41.316 kN. These are the same boundary conditions for the case of the 1.016-mm sheet with the S_1 tooling and the draw ratio of $R_L/R_A=1.7$. It is recalled that this case had the largest discrepancy between the experimental and theoretical results. The first two curves, (a) and (b), show the results found using the deformation theory of plasticity with a membrane and shell theory, respectively. Here it is seen that the bending terms and thickness distribution of the stress, both ignored in the membrane formulation, have the effect of raising the critical punch height. Altering the response of the material by changing the corner characteristics can further increase the critical punch height. Curves (c), (d), and (e) show the effects of different corner theories with no forward loading cone, $\theta_0=0$. As the unloading cone angle, θ_c, approaches $\pi/2$, the critical punch height increases. Flow theory is obtained when $\theta_c=\pi/2$. This case is examined, but no puckering instability is found regardless of the sheet thickness.

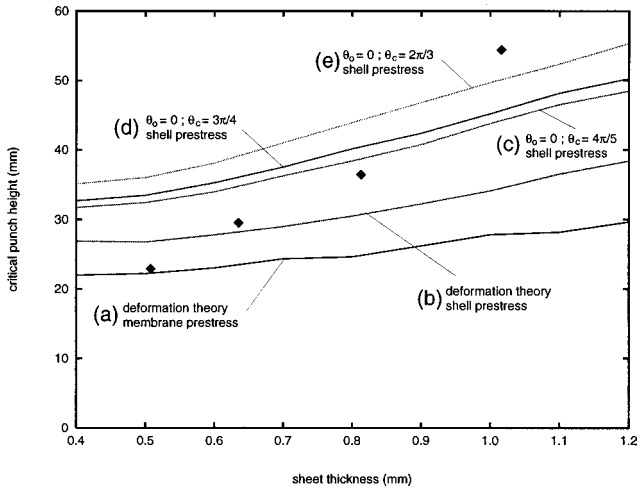

Fig. 5 Effect of sheet thickness on the critical punch height for a brass sheet with $R_L/R_A=1.7$, the S_1 tooling, BHF $=41.316$ kN a coefficient of friction $\mu=0.04$. The membrane prestress underpredicts the shell theory results for the same constitutive relations. Using a corner theory, and varying its corner geometry so as to approach a flow theory, the critical punch height increases. It is noted that the BHF used for all the numerical calculations is the experimental value corresponding to the thickest blank. Experimental results are marked by (♦).

Finally, the sensitivity of the results to the boundary conditions are examined by varying the coefficient of friction between the tooling surfaces and the sheet. The friction, combined with the BHF, supplies a restraining force on the sheet that prevents material from flowing into the die. The amount of material that flows into the die determines the compressive hoop stresses that cause puckering. Therefore, the coefficient of friction plays an important role in determining the critical punch height, as can be seen in Fig. 6. Once again the cases shown in Fig. 6 are variations of the case for the 1.016-mm sheet with the S_1 tooling and the draw ratio of $R_L/R_A=1.7$. The blank holder force for all the cases is 41.316 kN and the coefficient of friction is varied from 0.00 to 0.16. The effect of the coefficient of friction is greater for the shell theories (curves (b)–(e)) than for the membrane theory (curve (a)) as evidenced by the lower slope for the membrane theory curve. The effects for the different plasticity theories is the same for the shell theories since they have similar slopes. Looking at the region near the experimental results, $\mu=0.04$, it is seen that a slight change, say about 0.02, in the coefficient of friction can result in a change of up to 5 mm in the critical punch height. Therefore, it is determined that the boundary conditions (the coefficient of friction and BHF) have a very large effect on stability in the hemispherical cup test.

4 Conclusions

The general method proposed in Part I is applied to the modeling of the hemispherical cup test. The goal is to check how the method performs for different sheet thicknesses and to investigate the influence of simpler (membrane) prestress states versus more accurate (shell) prestress states.

As expected, better agreement with experimental results is obtained for thinner sheets using J_2 deformation theory of plasticity. As the sheet thickness increases, so does the discrepancy between the experimental results and the theoretical predictions. The main reason for this discrepancy is the presence in the principal solution of large deviations from proportional loading, which requires more sophisticated constitutive models (corner theories) to accurately predict the critical punch height.

In the application at hand, the minimum eigenvalue of the stability functional goes through zero at the onset of bifurcation, since a bifurcation type instability is guaranteed by the axisymmetry of the principal solution. For the general case of a nonaxisymmetric geometry, as for example for the punch test of noncircular blanks or blanks with some initial asymmetric imperfection, recent calculations done by the authors show that the minimum eigenvalue will not change sign at criticality. Consequently the onset of instability is not clearly defined, although it must still be connected to the minimum eigenvalue of the stability functional which measures the stiffness of the structure. Current work (unpublished) examines a nonaxisymmetric blank (a circular blank with a small initial imperfection) and a square blank deformed by a hemispherical punch and correlates the minimum eigenvalue with the initial appearance of surface wrinkles.

Acknowledgments

The partial support of ALCOA and NSF under grant G-CMS-9503956 are gratefully acknowledged. The encouragement of R. Stevenson (GM) during the course of this work are sincerely appreciated.

References

[1] Devons, J. D., 1941, *The Metallurgy of Deep Drawing and Pressing*, Chapman Hall, London.
[2] Triantafyllidis, N., 1985, ''Puckering Instability in the Hemispherical Cup Test,'' J. Mech. Phys. Solids, **33**, pp. 117–139.
[3] Donoghue, M., Stevenson, R., Kwon, Y. J., and Triantafyllidis, N., 1989, ''An Experimental Verification of the Hemispherical Cup Puckering Problem,'' ASME J. Eng. Mater. Technol., **111**, pp. 248–254.
[4] Triantafyllidis, N., and Samanta, S. K., 1986, ''Bending Effects on Flow Localization in Metallic Sheets,'' Proc. R. Soc. London, Ser. A, **406**, pp. 205–226.
[5] Christoffersen, J., and Hutchinson, J. W., 1979, ''A Class of Phenomenological Corner Theories of Plasticity,'' J. Mech. Phys. Solids, **27**, pp. 465–487.
[6] Goetz, A., 1970, *Introduction to Differential Geometry*, Addison-Wesley, New York.
[7] Hutchinson, J. W., 1974, ''Plastic Buckling,'' Adv. Appl. Mech., **14**, pp. 67–144.